Human-Centered Flood Mapping and Intelligent Routing through Augmenting Flood Gauge Data with Crowdsourced Street Photos

Bahareh Alizadeh, Ph.D. Student
Department of Construction Science, Texas A&M University, College Station, TX 77843, USA
Phone: 979-458-0182, E-mail: bahareh.alizadeh@tamu.edu

Diya Li, Ph.D. Student
Department of Geography, Texas A&M University, College Station, TX 77843, USA
Phone: 979-845-6523, E-mail: diya.li@tamu.edu

Julia Hillin, M.S. Student
Department of Geography, Texas A&M University, College Station, TX 77843, USA
Phone: 979-458-1096, E-mail: juliahillin@tamu.edu

Michelle A. Meyer, Associate Professor
Department of Landscape Architecture & Urban Planning, Texas A&M University, College Station, TX 77843, USA
Phone: 979-845-7813, E-mail: mmeyer@arch.tamu.edu

Courtney M. Thompson, Assistant Professor
Department of Geography, Texas A&M University, College Station, TX 77843, USA
Phone: 979-458-1096, E-mail: cthompson24@tamu.edu

Zhe Zhang, Assistant Professor
Department of Geography, Texas A&M University, College Station, TX 77843, USA
Phone: 979-845-6523, E-mail: zhezhang@tamu.edu

Amir H. Behzadan, Clark Construction Endowed Associate Professor *(corresponding author)*
Department of Construction Science, Texas A&M University, College Station, TX 77843, USA
Phone: 979-458-0182, E-mail: abehzadan@tamu.edu

Manuscript Submitted: Elsevier Journal of Advanced Engineering Informatics

Initial Submission: October 11, 2021

Revised Submission I: May 17, 2022

Human-Centered Flood Mapping and Intelligent Routing through Augmenting Flood Gauge Data with Crowdsourced Street Photos

ABSTRACT: The number and intensity of flood events have been on the rise in many regions of the world. In some parts of the U.S., for example, almost all residential properties, transportation networks, and major infrastructure (e.g., hospitals, airports, power stations) are at risk of failure caused by floods. The vulnerability to flooding, particularly in coastal areas and among marginalized populations is expected to increase as the climate continues to change, thus necessitating more effective flood management practices that consider various data modalities and innovative approaches to monitor and communicate flood risk. Research points to the importance of reliable information about the movement of floodwater as a critical decision-making parameter in flood evacuation and emergency response. Existing flood mapping systems, however, rely on sparsely installed flood gauges that lack sufficient spatial granularity for precise characterization of flood risk in populated urban areas. In this paper, we introduce a floodwater depth estimation methodology that augments flood gauge data with user-contributed photos of flooded streets to reliably estimate the depth of floodwater and provide ad-hoc, risk-informed route optimization. The performance of the developed technique is evaluated in Houston, Texas, that experienced urban floods during the 2017 Hurricane Harvey. A subset of 20 user-contributed flood photos in combination with gauge readings taken at the same time is used to create a flood inundation map of the experiment area. Results show that augmenting flood gauge data with crowdsourced photos of flooded streets leads to shorter travel time and distance while avoiding flood-inundated areas.

Keywords: Flood; crowdsourcing; artificial intelligence; floodwater depth; route optimization; emergency management.

1. INTRODUCTION

Urbanization, growing coastal population, climate change, and deforestation are the main drivers of increased flooding worldwide [1, 2, 3], and are expected to contribute to a tenfold increase in the annual flood loss over the next several decades (from $6 billion in 2005 to $60 billion in 2050) [4, 5]. Furthermore, rising global temperatures result in higher amounts of moisture retained in the atmosphere, which could lead to flooding in regions that have not experienced floods in the past [6]. The post-industrialization rise in the global mean sea level [7] has also led to more floods and storms. Currently, more than one billion people live in areas just 10 meters above high tide lines, which may be inundated in the near future due to changes in the hydrological cycle [8]. In Europe alone, more than 200 million people live in coastal regions (within 50 km from coastal lines) [9], and it is expected that a significantly larger population will be exposed to flood risks due to continued sea level rise and growing coastal population. Among European countries, the Netherlands has the highest relative population (58%) living in flood-prone areas [10]. Research also indicates that by 2100, at least 190 million people globally will experience flooding for the first time [8].

Of the 19% world population at risk of substantial flooding, 89% live in low and middle-income communities with undeveloped or poorly developed disaster risk management practices [10]. First responders and evacuees in these areas have limited access to accurate and timely flood risk information which hinders flood mitigation and preparedness [11]. Since flood risk management involves multiple stakeholder groups (e.g., residents, search and rescue teams, emergency managers, insurance companies), timely access to unified and reliable flood information is of the essence [12]. The anticipated elevated risk of flooding in many parts of the world also necessitates

innovative risk management approaches that can effectively navigate uncertainty, remove duplication, and utilize various publicly available resources and data [6].

Traditional approaches to flood mapping use in-situ flood sensors and stream gauges in or near bodies of water to monitor water levels, and consequently, extrapolate this information to estimate the extent of flooding in the surrounding areas. However, since these setups are primarily installed outside residential zones, obtained data may not fully reflect reshaped surface topography and microtopographic variations commonly seen in urban environments, ultimately yielding large estimation errors [13, 14]. For example, in a 2009 study, the comparison of elevation data extracted from the National Elevation Dataset (NED) and survey benchmarks yielded an error of 14.9 feet [15]. The main motivation of the research presented in this paper is to generate high spatial resolution flood maps for intelligent routing in and around residential neighborhoods by incorporating user-contributed flood photos with live stream flood gauge data. In achieving this goal, we are mainly interested in knowing whether complementary floodwater depth data obtained through the visual analytics of crowdsourced photos can help create accurate real-time information for flood inundation mapping. The central hypothesis of this study is that adding street-level floodwater depth data to existing flood gauge data will improve the quality of evacuation routing optimization. Our technical methodology is derived from the outcome of a community needs assessment survey that informs different aspects of technology design including a new crowdsourcing platform, named Blupix, used to integrate user-contributed photos with floodwater depth estimation models [16]. The effectiveness of this approach is assessed by carrying out route optimization on flood gauge data augmented with crowdsourced data.

In the remainder of this paper, first, a thorough review of the background of this research is conducted along three dimensions: community needs assessment, floodwater depth estimation

methodologies, and route optimization for finding flood-free evacuation routes. Next, a detailed description of the designed methodology is presented, followed by a case study using data from the 2017 Hurricane Harvey in Houston, Texas, to demonstrate the applicability of the proposed approach and assess model performance. Lastly, results are presented and discussed, conclusions are drawn, and limitations and future research directions are outlined.

2. BACKGROUND AND RESEARCH NEED

The review of the literature conducted in this section is organized into three parts: community needs assessment, floodwater depth estimation methodologies, and route optimization to find flood-free evacuation routes. Each part forms a critical step of the designed methodology in this research.

2.1. Community Needs Assessment

Effective communication of flood risks helps raise public awareness and plays a critical role in increasing community resilience against natural hazards [17, 18, 19, 20, 21, 22, 23, 24]. In this regard, having access to flood information and mitigation resources at multiple levels (e.g., educational content and training programs offered by state and local governments, reports and evidence collected by rescue teams and emergency managers, documented stories and lived experiences of residents in flood-prone areas) can contribute significantly to improved risk perception and communication [25, 26]. The means and the frequency by which people gather, access, process, and prioritize risk information influence how they make important decisions about sheltering, evacuation, and relocation during disasters [26, 27]. People's perceptions and expectations of disaster risks can also vary over time. For example, it was found that flood risk perception was significantly altered for some residents after being struck by severe flooding [28].

Traditionally, one-way risk communication from the authorities down to the public (i.e., experts informing residents of potential risks of natural hazards) has been used for alerting communities about flood risks. However, to promote trust in data and resulting policies and actions, recent research strongly favors two-way risk communication [29, 30], where members of the community actively participate in creating, sharing, and utilizing information about hazard risks, state of the environment affected by the hazard, and forthcoming decisions concerning sheltering, evacuation, and relocation [31]. Recently, various technologies have been used to develop disaster mitigation information systems. However, studies focusing on the technology acceptance model (TAM) in the context of disaster mitigation indicate that gaps still exist between the services provided by the system and the community's real needs [32, 33]. For example, as discussed by Thompson et al. [33], the implementation of most of the currently available decision support systems such as CEMPS (designed by [34] for damage assessment) and ARTEMIS (designed by]35, 36] for floods) is limited. Integrating community input in technology design can be a potential solution to the lack of acceptance of and trust in flood mitigation and risk communication technologies [36]. Crowdsourcing the data collection, for instance, can promote data transparency, as well as technology usefulness at the time of a disaster [37, 38, 39].

Another common approach to understanding community perception of involved risks is through conducting needs assessment surveys. Community surveys are used to study people's opinions and experiences about potential natural hazards. Researchers in New South Wales, Australia, for example, designed a community survey to identify factors influencing people's perception of flooding, and concluded that gender, age, proximity to rivers, and duration of living in flood-prone areas are the main influencers of low flood risk perception in many residents [40]. For example, it was found that the perception of the risk to property was greater for older people. Also, the lack

of awareness about flood risk was found to be higher in male respondents. In a 2010 study, a public survey was conducted in Boulder, Colorado to investigate how people perceive and react to flash flood warnings issued by the U.S. National Weather Service [41, 42]. Researchers found that approximately 75% of respondents trust flash flood warnings at least to some extent. However, even those who understood and noticed flash flood warnings were not completely aware of what preparatory actions to take after receiving such alerts. These and several other studies highlight the need for community-driven approaches to risk communication, evacuation planning, and hazard mitigation, rather than adopting "one-size-fits-all" solutions that may not fully consider the needs and priorities of the residents in affected areas.

2.2. Flood Depth Estimation Techniques

Over the years, various flood mapping systems have been proposed and developed by governments and scientific institutions [43]. In the U.S. and Canada, the Flood Damage Reduction Program (introduced in 1976) and the National Flood Insurance Program (introduced in 1968) were set up for flood mapping and mitigation [44, 45]. Following numerous flood events in the 1990s, large-scale flood mapping systems were developed in Europe [46]. For instance, in Germany and the U.K., flood maps are generated using data obtained from a network of monitoring stations installed near rivers and coasts. Current flood mapping systems use gauge data, hydraulic and hydrologic models [47, 48, 49], light detection and ranging (LiDAR) [50, 51], radar-based precipitation depths, synthetic aperture radar (SAR) images, advanced streamflow measurement [52], digital elevation model (DEM) with an X-band sensor, and short-wavelength microwaves transmitted by satellites [53]. Among these methods, aerial imagery and DEM models may not provide accurate data in developing areas and places where vegetation and urban structure are dense because of surface variability [54]. Moreover, adverse weather and shaded areas impose restrictions for

overhead imagery [55, 56]. Hydraulic and hydrologic models are also sensitive to data inconsistency, modeling uncertainty, and miscalibration [52, 57]. Furthermore, resulting data might not be readily available to the public [58]. On the other hand, conventional gauge and sensor data are primarily available for fixed stations in close vicinity to riverine and coastal areas, which is hindersome to effective evacuation planning and search and rescue missions, considering the low granularity of derived flood data relative to the high spatial resolution of the road network [3, 47].

With advancements in computer vision, researchers have attempted to analyze flood-related images and videos for estimating the water depth using omnipresent measurement benchmarks. For example, Chaudhary et al. [59] compared detected submerged objects in images with reference objects (e.g., average human height). The main source of error for this approach was that the distance between cameras and objects (i.e., depth effect) was not considered. Park et al. [60] analyzed and compared photos of submerged vehicles with the most similar 3D generated vehicles, allowing them to estimate the flood depth with a mean absolute error (MAE) of 2.5 inches. Hao et al. [61] used computer vision models to analyze the spatiotemporal progress of urban floods from surveillance videos. These methods, however, rely on analyzing images of measurement benchmarks with different shapes and forms (e.g., vehicles, fire hydrants, bicycles, trees) by assuming predefined sizes for these objects. A more generalizable approach, however, should rely on measurement benchmarks which not only are omnipresent in urban areas and road segments, but also have regulated and standardized sizes and shapes in many geographical regions. Informed by this gap, Alizadeh Kharazi and Behzadan [62] proposed a flood depth estimation approach using stop signs as measurement benchmarks, due to their standardized shape and size. They used conventional image processing techniques to analyze photos of stop signs prior to and after floods,

and determined floodwater depth with an MAE of 12.63 inches. Alizadeh et al. (2021) later adopted a similar method for flood mapping and evacuation route planning using Geographic Information System (GIS) [3]. Building on our previous work, in this paper we utilize object detection as a faster and more accurate method for flood depth estimation.

More recently, various forms of deep convolutional neural networks (CNNs) have been introduced for high-accuracy object detection in photos and videos. These models can be used to detect objects of interest (e.g., traffic signs, vehicles, people) in flood photos and make inferences about the depth of floodwater. Object detection models such as Single Shot Detector321 (SSD321) [63], Deconvolutional Single Shot Detector321 (DSSD321) [64], RetinaNet-101-500 [65], and Region-based Fully Convolutional Networks (R-FCN) yield mean average precision (mAP) of 45.4% with 16 frames per second (FPS), 46.1% with 12 FPS, 53.1% With 11 FPS, and 51.9% with 12 FPS on the Microsoft COCO dataset [66], respectively. The You-Only-Look-Once (YOLO) model, that was proposed by Redmon et al. [67], uses a single neural network to predict bounding boxes and class probabilities in one round of image evaluation, enabling object detection in near real-time with high accuracy. The latest official version of the YOLO model by the date of this study, i.e., YOLOv4 [68], achieves 65.7% mAP with 65 FPS on the Microsoft COCO dataset. The performance of this model surpasses previous versions by 10% in AP, and 12% in FPS, primarily due to enhanced feature extraction enabled by the cross-stage-partial-connections network (CSP) with the Darknet-53 CNN [69], along with spatial pyramid pooling (SPP) for filtering important features, and the addition of PANet [70], a path aggregation network aimed at more efficient parameter aggregation.

2.3. Route Optimization for Wayfinding in Flood Events

Evacuation planning is a major component of flood management as it guides the movement of people and goods from at-risk places to safe areas [71 ,72]. In recent studies, optimization- and simulation-based models have been used for evacuation routing [73]. Flood evacuation has been increasingly recognized as being a critical component of disaster management adaptation to floods [74]. Previous research has particularly focused on formalizing the evacuation process into different stages including the warning stage, withdrawal stage, and shelter stage, and finding separate solutions to each stage [74, 75]. However, recent research by Insani et al. [75] shows that complex evacuation solutions may not work well in no-notice or short-notice evacuation situations that could occur immediately after a disaster strikes. As there is only limited information (e.g., velocity and spread of floodwater movement) within a short response time, researchers have also considered interpolation techniques [76, 77] or buffer decay function [78] to compensate for limited data and support large-scale flood mapping. To date, however, the literature on interpolation techniques for flood mapping in real-world route optimization scenarios is limited. Stepanov and Smith [72] utilized multi-objective route optimization and M/G/C/C state-dependent queuing networks to minimize travel time, distance, and traffic delays. In another study, single-objective optimization and evacuation simulation were used to maximize the number of evacuees and minimize travel time during flood events [79]. Researchers have also utilized route optimization and CPLEX, a high-performance optimization software, to optimize evacuation time and route for no-notice evacuation of transit-dependent citizens [80].

The routing problem is one of the most studied combinatorial optimization problems, first mentioned in 1959 as the *truck dispatching problem* to determine an optimal route for a fleet of gasoline delivery trucks between a terminal and several service stations [81]. One important variant of the routing problem is emergency evacuation planning [82], which aims to evacuate

205 residents from a hazard-inundated region to a safe place in the shortest possible time and on the
206 safest path. A recent work by Alizadeh et al. [3] considered a distance decay function to generate
207 flood depth maps and conduct routing using the A* search algorithm [83]. To overcome data
208 scarcity in the experiment scenario, the distance decay function applied a Gaussian buffering
209 function to approximate floodwater depth in areas surrounding a point with field-verified
210 floodwater depth reading. Previous work has utilized various interpolation methods to map flood
211 hazard. Berens et al. [84], for instance, used the inverse distance weight method to plot the flood
212 map in a riverine area. Another common way to plot a flood map is the kriging interpolation
213 method [85, 86, 87]. For example, Nezhad et al. [88] used residual kriging with flood gauge data
214 to estimate regional flood frequency. In another study, Zhang et al. [89] used empirical Bayesian
215 kriging to interpolate ground pixels for mapping the digital terrain model (DTM) for flood
216 vulnerability mapping.

217 ## 3. METHODOLOGY

218 As shown in Figure 1, the designed methodology in this research consists of four steps, namely
219 conducting a community needs assessment survey, designing an evacuation decision support
220 platform based on the identified needs, creating enhanced flood depth maps using multiple data
221 sources, and using enhanced flood depth data for risk-informed route optimization. In this section,
222 first a brief description of a community needs assessment survey, that was conducted to inform the
223 research design, is presented. Next, the design approach to developing an evacuation decision
224 support platform followed by an enhanced flood depth mapping system using multiple data sources
225 is described. The system uses paired pre- and post-flood stop sign photos to estimate the depth of
226 floodwater, and consequently uses this information to carry out risk-informed route optimization.

227 ***Figure 1.*** *Key steps of the designed methodology.*

3.1. Conducting a Community Needs Assessment Survey

To effectively incorporate user input into technology design and validation, we first conducted a needs assessment survey in local communities in Houston and Galveston, Texas, that are among the most vulnerable to flood risk in the U.S. Stakeholder involvement ensures that the designed technology and tools have a high degree of practicality among intended users [90], while also helping improve the quality, functionality, and ease of use of the developed tools, resulting in increased user satisfaction of the research outcomes [91]. Survey respondents were recruited using snowball sampling by sharing the survey link with several community partners and distributing the survey on social media, university email lists, and local outlets. The survey asked respondents to share their past experiences with flooding and rescue operations, and describe the types of information that would have helped them make rescue and evacuation decisions. Survey data were collected via Qualtrics, an online survey application, and included both closed-ended and open-ended questions. Quantitative data were analyzed using descriptive statistics, and qualitative data from the open-ended questions were analyzed by developing codes and combining them into themes [92].

The sample results (n = 217) identified several types of information that could enhance the evacuation experience. Both residents and rescue responders stated a need for more accurate flood and route information, as well as access to field data to improve their ability to make decisions during a flood event. Residents focused on more accurate flood data (e.g., flood severity, water level rise) and evacuation information (e.g., traffic conditions, evacuation routes). They also indicated a need for real-time rescue and response efforts and coordination, as well as floodwater conditions. Similarly, rescuers identified a need for real-time floodwater conditions and rescue operations (e.g., rescue progress and completion), in addition to more accurate flood information.

However, rescuers' needs were centered on where to take evacuees, how to transport them to safe places, built environment conditions (e.g., submerged house, debris), and various flood indicators (e.g., water speed, flood depth).

Following the administration of this Qualtrics survey, and in lieu of in-person community meetings with local stakeholders (which was hampered due to the COVID-19 pandemic), we hosted three virtual discussions with civilian and rescue operator stakeholders. In particular, we coordinated two virtual discussions with nonprofit organizations that conduct volunteer search and rescue activities in flood and coastal storm events. Each event included 3-6 rescue volunteers who described their information needs and technology use during flood rescue operations. We also hosted a public event attended by 15 people to discuss the tool development and flood needs.

3.2. Designing an Evacuation Decision Support Platform Based on the Identified Needs

Based on the identified community needs, we developed a crowdsourcing application, named Blupix, using web-based GIS. The backbone of this platform is a CNN architecture that estimates the depth of floodwater in user-contributed photos by detecting stop signs and comparing pole lengths in pre- and post-flood photos of the same sign. Figure 2 illustrates the graphical user interface of Blupix, which gives users the ability to upload images of flooded stop signs, and view previously uploaded photos that are either paired (with corresponding pre-flood images of the same sign) or unpaired. Each photo pair also displays the calculated floodwater depth at the location of the stop sign.

Figure 2. *The graphical user interface of the Blupix crowdsourcing application.*

To host the Blupix application, we developed an advanced cyberinfrastructure using container technology. As shown in Figure 3, we used the Model View Controller (MVC) software design pattern, where the *View* displays information (e.g., user profile, flood information, collected stop sign images), and the *Controller* processes the users' connection. The user interface is developed

using a modern front-end framework named React J.S. (a.k.a., React). Once the React application is developed and ready to deploy, a Webpack middleware is designed to bundle the entire system to a set of static assets, significantly reducing loading time on the browser for viewing the application [93]. Unlike traditional web development technologies such as HTML and JavaScript, React supports large and complex web development with seamless data manipulation without subsequent page refreshes when users view dynamic pages [94].

Figure 3. *The Model View Controller (MVC) framework of the Blupix crowdsourcing application.*

Except for back-end and front-end modules deployed on a Kubernetes Cluster, we adopted several cloud-native services to support the application development (Figure 4). The front-end components construct the requests made by users and send them to the Google Cloud Platform (GCP). Next, the components render the user interface based on the response received from GCP. A PostgreSQL database is designed to support a back-end server to store relational data (e.g., user profile, flood height, flood date). However, non-relational data in the image cannot be easily stored in PostgreSQL. Thus, after converting the image data to binary data, we integrated Microsoft Azure to store large amounts of unstructured pre-flood and post-flood data. The last part of this software architecture consists of a Docker Hub to mount the code. With this image library, we built our development automation workflow to speed up the application deployment.

Figure 4. *Illustration of the system architecture of the Blupix crowdsourcing application.*

3.3. Creating Enhanced Flood Depth Mapping Using Multiple Data Sources

3.3.1. Floodwater depth estimation from paired stop sign photos

As previously mentioned, in this study, the objects of interest for flood depth estimation in street photos are submerged stop signs. By comparing the height of a stop sign pole before and during a flood event, an estimate of the depth of floodwater at the location of the stop sign can be made. In many parts of the world, traffic signs are regulated and have standardized shapes, colors, and

dimensions. In North America, for example, the octagon shape of a stop sign has a width and a height of 30 inches and 36 inches on single-lane and multilane roads and expressways, respectively [95]. However, sign poles have various lengths based on the traffic load and the characteristics of the road where they are mounted. As Figure 5 illustrates, a constant ratio can be calculated by dividing the actual size of the stop sign (in inches) by the detected size of the same sign (in pixels). This ratio is then used to estimate the pole length in inches. Conducting this operation for paired pre- and post-flood photos of the same stop sign will yield the overall pole length (P) as well as the above-the-water pole length (P', the portion of the pole that is not submerged in water). The difference between these two lengths is an estimate of the depth of floodwater at the location of the stop sign (D).

Figure 5. *Flood depth estimation using paired pre- and post-flood photos of a stop sign.*

A customized YOLOv4 object detection model is adopted to size stop signs and poles in photos, and count the number of pixels corresponding to the width and height of detected objects. The network architecture of this model comprises a backbone for extracting the main features of the input image, a head that is trained to detect specific objects of interest, and a neck which processes extracted features (Figure 6). The model output consists of detected bounding boxes with confidence scores along with associated classes. For best performance, the model is pre-trained on 80 classes from the Microsoft COCO dataset, including stop signs. Since the original YOLOv4 model is not trained to detect poles, transfer learning is used for training the model for pole detection without losing previously learned general features. To this end, pre-trained weights of all layers are frozen, except for the last three YOLO layers which are fine-tuned using the new training set. The training set consists of 334 post-flood photos (web-mined), 334 pre-flood photos (extracted from the Microsoft COCO dataset), as well as 61 pre-flood and 71 post-flood web-mined zero label photos of other traffic signs. Furthermore, since stop signs appear large enough

in most of the images, the standard network resolution of the YOLO model is reduced from 416 × 416 to 320 × 320. While this lower resolution does not compromise the quality of stop sign and pole detection, it lowers the computational cost of the training process.

Figure 6. *The architecture of YOLOv4 modified for detecting stop signs and their poles in photos.*

Training is initially performed for 4,000 iterations, five complete epochs, and using a learning rate of 0.001, Adam optimizer [96], batch size of 1, and subdivision of 64. Moreover, random and real-time data augmentation is utilized to increase the size of the training set by creating slightly modified copies of existing images (through changing hue, saturation, exposure, horizontal flipping, or adding mosaic filters) [68]. Training time is approximately 12 hours with an average loss of 0.567 on a Lenovo ThinkPad laptop computer with 7 cores, 9750H CPU, 16 GB RAM, and Nvidia Quadro T1000 GPU with a 4 GB memory. To prevent overfitting (inability to generalize well to new data), 5-fold cross-validation is utilized by dividing the training set into five subsets, each constituting 20% of randomly selected (but mutually exclusive) images from the training set. The model is then trained five times on four subsets and validated on the remaining subset. The mAP of the model is calculated as the average of all five computed mAPs across all validation sets. Finally, the model is trained on the training set with the optimum number of iterations (calculated as 3,000 before overfitting is observed) and further tested with unseen data.

3.3.2. Performance of the object detection model

To measure the performance of the YOLOv4 model, ground-truth information is generated by manually labeling pre- and post-flood photos for objects of interest (i.e., stop signs, poles). For each detection, Equation 1 is used to calculate the intersection over union (IoU) considering the pixel overlap between the predicted bounding box (B') and the ground-truth bounding box (B). A threshold IoU value of 50% is adopted to differentiate between true and false detections, and

subsequently calculate precision and recall for each object class. The AP for each class is determined as the area under the precision (the proportion of detected positive cases that are real positives) and recall (the proportion of real positive cases that are identified as positive) curve (Equation 2). Finally, mAP is computed from the AP of all individual classes, as formulated in Equation 3.

$$IoU = \frac{B' \cap B}{B' \cup B} \quad \text{Equation 1}$$

$$AP = \frac{1}{N} \sum_{i=1}^{N} P\Delta r_i \quad \text{Equation 2}$$

$$mAP = \sum_{i=1}^{N} AP_i \quad \text{Equation 3}$$

3.4. Using Enhanced Flood Depth Data for Risk-Informed Route Optimization

In this step, the Dijkstra routing algorithm [97] is applied to calculate a flood-free evacuation route. To this end, a flood risk map is first built for route optimization by overlaying gauge data with floodwater depth data. Generally, values between two closely located points can be predicted through point interpolation. The accuracy of this interpolation, however, is affected by the sparseness of the interpolation points. Using stop sign points in addition to gauge data can enhance the density of interpolation observations. We use Empirical Bayesian Kriging (EBK) [98] as a geospatial interpolation method to generate a flood risk map for route optimization. EBK is different from other kriging methods as it reduces the tendency to attain the overall mean value of variables and allows large deviations for predicted values over space [99]. Spatial autocorrelation (i.e., increasing similarity of spatial features with decreasing distance) is assumed in all geostatistical methods [100]. Particularly, we utilize EBK with semivariogram to evaluate the diminishing similarity among flood data points over distance [99]. Equation 4 is used to interpolate flood depth values for gauge points and stop sign points using the EBK method with a power

semivariogram model. In this Equation, h is the distance, a and b are positive constant parameters, and n denotes the parameter of nugget effect as an intercept of variogram function.

$$\gamma(h) = n + b|h|^a \quad \text{Equation 4}$$

The parameters in Equation 4 are estimated by restricted maximum likelihood (REML) [98]. According to the EBK implementation by Krivoruchko et al. [98], the main kriging method can be simplified as in Equation 5, where K denotes the number of observation points, z_i is the observation point in location s_i, $y(s_i)$ is the transformed Gaussian in the same location, ϵ_i is the normally distributed measurement error of z_i, and function $t(\cdot|\Theta)$ is a transformation to Gaussian process with parameter Θ. EBK estimates the semivariogram through repeated simulations of residuals [101].

$$z_i = t^{-1}(y(s_i) + \epsilon_i|\Theta) = z(s_i) + {\epsilon_i}^2, \qquad i = 1 \dots K \quad \text{Equation 5}$$

4. RESULTS AND DISCUSSION

To demonstrate the applicability of the proposed methodology, we select 20 paired photos, uploaded on the Blupix app, that were taken during Hurricane Harvey (August 27 – September 1, 2017) in Houston, Texas. These photo pairs are then analyzed by the trained YOLOv4 model for floodwater depth estimation. In addition to stop sign data, we also leverage gauge data to compute flood depth for the areas without paired stop sign photos, and to demonstrate our interpolation method and routing algorithm. The gauge height (a.k.a., stage) is the height of the water in the stream above a reference point, and refers to the water surface elevation in the specific pool or low-lying terrain near the gauge station. For our experiment area, the gauge records in all 1,321 gauge stations in Texas are scraped via the National Weather Service [102]. The average gauge height is calculated by comparing the gauge heights during Hurricane Harvey and the annual mean gauge heights of other years during the same time period of August 27 to September 1, 2017.

4.1. Floodwater Depth Estimation Using Stop Sign Data

The mAP of the model on the validation set is calculated as 97.04%, by taking the average mAP in each of the five training sets. The optimum number of iterations obtained (when the highest mAP is achieved) is 3,000, which is equal to the average number of optimum iterations in the five training sets. The average precision of the model on test data (20 paired photos) is calculated as 100% and 96.54% for the stop sign and pole classes, respectively. The MAE for floodwater depth estimation is 3.80 in. Results are summarized in Table 1.

Table 1. *Performance of the trained YOLOv4 model on 20 selected paired photos in Hurricane Harvey (August 27 – September 1, 2017) in Houston, Texas. (S=stop sign; P=pole)*

4.2. Flood Map augmentation Using Stop Sign Data in addition to Gauge Data

Using ArcGIS API for Python [103], a comparison experiment is created with gauge only and gauge + stop sign floodwater depth data. We use contour lines to represent variations in interpolated flood depth values. We assume the changes between those contour line intervals to be consistent, where each class follows a geometric series with approximately the same number of interpolated flood depths. Figure 7 demonstrates the distribution of stop sign points and gauge points used in this experiment.

Figure 7. *Location of start and end points (black pins), flood gauges (green squares), and stop sign points (red circles) in the experiment area.*

Figure 8(a) shows the calculated route under the non-flood scenario obtained by regular Dijkstra routing, while Figure 8(b) and Figure 8(c) show optimized evacuation paths with flood depth consideration using EBK and Dijkstra algorithms simultaneously. For best comparison, Figure 8(b) is calculated with only flood gauge data, and Figure 8(c) shows the resulting route when stop sign data is added to flood gauge data. To ensure date/time consistency between flood gauge data

and stop sign data, we use time information retrieved from metadata of flooded stop sign photos to query flood gauge data [102]. The highlighted blue polygons in Figure 8 represent the estimated flooded area, and thick dark blue lines represent suggested routes under no-flood and flood scenarios. Using a 100-inch distance threshold for avoiding flooded areas, the optimized evacuation path with only gauge data, shown in Figure 8(b), conservatively detours several potentially high flood risk areas before reaching the destination safely. In contrast, the route shown in Figure 8(c) generated using the EBK method is a shorter (yet still safe) alternative. Table 2 compares the three routes considering the estimated travel time (driving) and distance obtained using ArcGIS API. Each column represents a routing scenario corresponding to Figures 8 (a), (b), and (c). As shown in this Table, using only gauge data will increase the user's travel time and distance, possibly exposing them to more flood risk over time (since floodwaters move).

Figure 8. *Flood mapping and risk-informed evacuation route optimization using EBK and Dijkstra algorithms: (a) regular route planning with Dijkstra algorithm; (b) EBK method with Dijkstra algorithm using only flood gauge data; (c) EBK method with Dijkstra algorithm using flood gauge data and stop sign data.*

Table 2. *Comparison of three routing scenarios in the experiment area.*

5. CONCLUSION

The number and intensity of flood events is expected to increase globally due to asymmetric urbanization, growing coastal population, and climate change. During urban floods, emergency managers, search and rescue teams, and evacuees make decisions based on available data, which may not necessarily represent how floodwaters move in the surrounding areas, especially in and around residential neighborhoods. With the goal of improving the quality of decisions made during flood events to evacuate people or move goods and services while avoiding flooded areas, this

437 study first conducted a community needs assessment that highlighted the need for (near) real-time
438 data on floodwater conditions, risk-informed evacuation plans, and safe and shortest transit routes.
439 To address these needs, a decision support system was subsequently developed which utilized
440 crowdsourced photos of submerged stop signs to generate street-level flood maps with high spatial
441 resolution (compared to flood gauge data), and develop risk-informed evacuation plans during
442 flood events. The designed floodwater depth estimation method compared photos of submerged
443 stop signs with photos of the same stop signs before the flood. To enable crowdsourced data
444 collection, a web application, called Blupix, was designed and launched. Images collected by the
445 Blupix app were analyzed using a customized version of the YOLOv4 model that was pre-trained
446 on the Microsoft COCO dataset and re-trained on an in-house dataset of stop sign images. This
447 model was deployed to calculate floodwater depth as the difference between sign pole lengths in
448 pre- and post-flood photos. The advantage of using stop signs as measurement benchmarks is that
449 their shapes and sizes are standardized, and a large number of these signs are installed and easily
450 recognizable in urban areas (compared to the relatively fewer number of conventional flood
451 gauges). Finally, a route optimization algorithm was implemented based on the generated
452 inundation map to determine the shortest flood-free evacuation route.
453 To evaluate the efficacy of the designed approach, 20 paired pre- and post-flood photos of stop
454 signs from Hurricane Harvey (2017), in Houston, Texas were selected. The mAP and the average
455 detection time of the model on the test data were 98.27% and 0.10 seconds, respectively. Route
456 optimization was first implemented on gauge data. This was followed by generating a flood map
457 using gauge + stop sign floodwater depth data. Results indicated the effectiveness of the proposed
458 method in determining shorter transit routes during flood events compared to the routes generated
459 based on gauge data only.

A key challenge in using crowdsourced data for flood mapping is that technology users might upload incorrect photos [104]. In this study, to remedy potential cases where user-contributed photos are not of expected quality, all image uploads were initially inspected by trained project personnel (a.k.a., app admin), prior to being approved or rejected. Only approved photos were shown on the map. The second challenge is the timeliness of pairing pre- and post-flood photos on the Blupix app. To overcome this challenge and facilitate data collection at scale, the authors are currently designing a computationally lighter version of the object detection model and an easy-to-use user interface that can run on consumer-grade mobile devices, thus enabling geographically dispersed users to assist not only in capturing new post-flood photos of submerged stop signs but also in pairing previously uploaded photos of submerged stop signs with corresponding flood-free views of the same signs. The mobile app will allow the user to either take a geotagged photo at the location of the stop sign or find a pre-flood view of the same stop sign on online mapping systems (e.g., Google Street View). The envisioned user interface and interaction features will ultimately expedite the calculation and increase the spatial resolution of floodwater depth, while supporting personalized, risk-informed route optimization based on user attributes (e.g., age, disability status) and preferences (e.g., points of interest), as well as evacuation resources (e.g., type of vehicle).

Additionally, using an interpolation method for flood mapping could be challenging given the spatial disparity of stop signs and gage stations, which may affect interpolation results [105]. Besides increasing the size of the user pool to improve the quality and representativeness of stop sign flood depth data, as part of the future work of this study, we will explore the possibility of integrating well-established hydrological models [106, 107] to compensate for geographical regions with uneven data distribution. In rural areas that lack both stop sign and gauge data, it

would be also possible to explore the usage of remote sensing data as a supplement to support flood mapping with interpolation [108].

6. ACKNOWLEDGMENTS

This study is funded by award #NA18OAR4170088 from the National Oceanic and Atmospheric Administration (NOAA), U.S. Department of Commerce. We would also like to acknowledge the support of Mr. Greg Spiller and Mr. Chris Mouchyn (College of Geosciences IT professionals at Texas A&M University) for hosting the Blupix application on the web (https://blupix.geos.tamu.edu). In addition, we would like to thank Mr. Nathan Young (undergraduate student at Texas A&M University) for his assistance in data collection. Any opinions, findings, conclusions, and recommendations expressed in this paper are those of the authors and do not necessarily represent the views of the NOAA, Department of Commerce, or the individuals named above.

7. LIST OF REFERENCES

[1] V. Sahin, M. J. Hall (1996), The effects of afforestation and deforestation on water yields, Journal of Hydrology 178 (1–4) 293–309, Available from <https://doi.org/10.1016/0022-1694(95)02825-0>

[2] K. Bjorvatn (2000), Urban infrastructure and industrialization, Journal of Urban Economics 48 (2) 205–218, Available from <https://doi.org/10.1006/juec.1999.2162>

[3] B. Alizadeh, D. Li, Z. Zhang, A. H. Behzadan (2021), Feasibility study of urban flood mapping using traffic signs for route optimization, Proceeding of EG-ICE 2021 Workshop on Intelligent Computing in Engineering 572-581, Available from <https://arxiv.org/abs/2109.11712>

[4] E. Mills (2005), Insurance in a climate of change, Science 309 (5737) 1040-1044, Available from <https://doi.org/10.1126/science.1112121>

[5] N. W. Arnell, B. Lloyd-Hughes (2014), The global-scale impacts of climate change on water resources and flooding under new climate and socio-economic scenarios, Climatic Change 122 (1) 127-140, Available from <https://doi.org/10.1007/s10584-013-0948-4>

[6] World Bank Group (2021), Floods and droughts: An epic response to these hazards in the era of climate change, Available from <https://www.worldbank.org/en/news/feature/2021/06/17/floods-and-droughts-an-epic-response-to-these-hazards-in-the-era-of-climate-change>

[7] R. E. Kopp, A. C. Kemp, K. Bittermann, B. P. Horton, J. P. Donnelly, W. R. Gehrels, S. Rahmstorf (2016), Temperature-driven global sea-level variability in the Common Era, Proceedings of the National Academy of Sciences 113 (11) E1434-E1441. Available from <https://doi.org/10.1073/pnas.1517056113>

[8] S. A. Kulp, B. H. Strauss (2019), New elevation data triple estimates of global vulnerability to sea-level rise and coastal flooding, Nature Communications 10 (1) 1-12, Available from <https://doi.org/10.1038/s41467-019-12808-z>

[9] M. I. Vousdoukas, L. Mentaschi, J. Hinkel, P. J. Ward, I. Mongelli, J. C. Ciscar, L. Feyen (2020), Economic motivation for raising coastal flood defenses in Europe, Nature Communications 11 (1) 1-11, Available from <https://doi.org/10.1038/s41467-020-15665-3>

[10] J. Rentschler, M. Salhab (2020), People in Harm's Way: Flood exposure and poverty in 189 countries, Policy Research Working Paper 9447, World Bank, Washington DC, Available from <http://hdl.handle.net/10986/34655>

527 [11] J. D. Paul, B. Wouter, A. Simon, J.A. Ballesteros-Cánovas, J. Bhusal, K. Cieslik, J. Clark, S.
528 Dugar, D.M. Hannah, M. Stoffel, A. Dewulf (2018), Citizen science for hydrological risk
529 reduction and resilience building, Wiley Interdisciplinary Reviews: Water 5 (1) e1262,
530 Available from <https://doi.org/10.1002/wat2.1262>
531 [12] T. Mai, S. Mushtaq, K. Reardon-Smith, P. Webb, R. Stone, J. Kath, D. A. An-Vo (2020),
532 Defining flood risk management strategies: A systems approach, International Journal of
533 Disaster Risk Reduction 47 101550, Available from
534 <https://doi.org/10.1016/j.ijdrr.2020.101550>
535 [13] S.W. Lo, J.H. Wu, F.P. Lin, C.H. Hsu (2015), Visual sensing for urban flood monitoring.
536 Sensors 15(8) 20006-20029, Available from <https://doi.org/10.3390/s150820006>
537 [14] S. Dong, T. Yu, H. Farahmand, A. Mostafavi (2021), A hybrid deep learning model for
538 predictive flood warning and situation awareness using channel network sensors data,
539 Computer-Aided Civil and Infrastructure Engineering 36(4) 402-420, Available from
540 <https://doi.org/10.1111/mice.12629>
541 [15] D. R. Maidment (2009), FEMA flood map accuracy, In World Environmental and Water
542 Resources Congress 2009: Great Rivers 1-10, Available from
543 <https://doi.org/10.1061/41036(342)492>
544 [16] Blupix Application (2021), Available from <https://blupix.geos.tamu.edu>
545 [17] P. Brown, A. J. Daigneault, E. Tjernström, and W. Zou (2018), Natural disasters, social
546 protection, and risk perceptions, World Development 104 310–325, Available from
547 <https://doi.org/10.1016/j.worlddev.2017.12.002>
548 [18] P. D. Nunn, W. Aalbersberg, S. Lata, M. Gwilliam (2014), Beyond the core: Community
549 governance for climate-change adaptation in peripheral parts of Pacific Island Countries,

Regional Environmental Change 14 221-235, Available from <https://doi.org/10.1007/s10113-013-0486-7>

[19] J. Tyler, A. A. Sadiq (2018), Friends and family vs. government: who does the public rely on more to prepare for natural disasters?, Environmental Hazards 17 (3) 234–250, Available from <https://doi.org/10.1080/17477891.2018.1425204>

[20] J. C. Beggs (2018), Applications: Disaster communication and community engagement., disaster epidemiology, Academic Press 163–169, Available from <https://doi.org/10.1016/B978-0-12-809318-4.00022-8>

[21] J. Becker, D. Johnston, M. Coomer, and K. Ronan (2008), Flood risk perceptions, education and warning in four communities in the Hawkesbury-Nepean Valley, New South Wales, Australia, results of a questionnaire survey, February 2006, CQUniversity, Journal contribution 2008(2) 1-58, Available from <https://hdl.handle.net/10018/31560>

[22] J. P. Reser, G. L. Bradley, A. I. Glendon, M. C. Ellul, and R. Callaghan (2015), Public risk perceptions, understandings and responses to climate change, Applied Studies in Climate Adaptation 43-50, Available from <http://hdl.handle.net/10072/49216>

[23] M. Buchecker, G. Salvini, G. D. Baldassarre, E. Semenzin, E. Maidl, and A. Marcomini (2013), The role of risk perception in making flood risk management more effective, Natural Hazards and Earth System Sciences 13 3013–3030, Available from <https://doi.org/10.5194/nhess-13-3013-2013>

[24] S. Fuchs, K. Karagiorgos, K. Kitikidou, F. Maris, S. Paparrizos, T. Thaler (2017), Flood risk perception and adaptation capacity: A contribution to the socio-hydrology debate, Hydrology and Earth System Sciences 21(6) 3183-3198, Available from <https://doi.org/10.5194/hess-21-3183-2017>

573 [25] D. Fitzpatrick-Lewis, J. Yost, D. Ciliska, S. Krishnaratne (2010), Communication about
574 environmental health risks: A systematic review, Environmental Health 9 (11-15), Available
575 from <https://doi.org/10.1186/1476-069X-9-67>
576 [26] G. T. Sansom, K. Aarvig, L. Sansom, C. Thompson, L. Fawkes, A. Katare (2021),
577 Understanding risk communication and willingness to follow emergency recommendations
578 following anthropogenic disasters, Environmental Justice 14 (2) 159-167, Available from
579 <https://doi.org/10.1089/env.2020.0050>
580 [27] M. K. Lindell, R. W. Perry (2004), Communicating environmental risk in multiethnic
581 communities, Sage Publications, Available from
582 <https://dx.doi.org/10.4135/9781452229188>
583 [28] P. Brown, A. J. Daigneault, E. Tjernström, W. Zou (2018), Natural disasters, social
584 protection, and risk perceptions, World Development 104 310-325, Available from
585 <https://doi.org/10.1016/j.worlddev.2017.12.002>
586 [29] P. Bennett, K. Calman, S. Curtis, D. Fischbacher-Smith (Eds.) (1999), Understanding
587 responses to risk: some basic findings, Risk Communication and Public Health, Oxford
588 University Press 3-19, Available from
589 <https://doi.org/10.1093/acprof:oso/9780199562848.001.0001>
590 [30] J. A. Bradbury (1994), Risk communication in environmental restoration programs, Risk
591 Analysis 14 357-363, Available from <https://doi.org/10.1111/j.1539-
592 6924.1994.tb00252.x>
593 [31] R. Alsnih, P. R. Stopher (2004), Review of procedures associated with devising emergency
594 evacuation plans, Transportation Research Record 1865 (1) 89-97, Available from
595 <https://doi.org/10.3141/1865-13>

596 [32] T. Siswanto, R. Shofiati, H. Hartini (2018), Acceptance and utilization of technology
597 (UTAUT) as a method of technology acceptance model of mitigation disaster website, In
598 IOP Conference Series: Earth and Environmental Science 106(1) 012011, IOP Publishing,
599 Available from <http://doi.org/10.1088/1755-1315/106/1/012011>
600 [33] S. Thompson, N. Altay, W. G. Green III, J. Lapetina (2006), Improving disaster response
601 efforts with decision support systems, International Journal of Emergency Management 3(4)
602 250-263, Available from
603 <https://www.inderscienceonline.com/doi/abs/10.1504/ijem.2006.011295>
604 [34] J.Z. Hernandez, J.M. Serrano (2001), Knowledge-based models for emergency management
605 systems, Expert Systems with Applications 20(2) 173–186, Available from
606 <https://doi.org/10.1016/S0957-4174(00)00057-9>
607 [35] F.N. de Silva, R.W. Eglese (2000), Integrating simulation modeling and GIS: spatial decision
608 support systems for evacuation planning, Journal of the Operational Research Society 51(4)
609 423–430, Available from <https://doi.org/10.1057/palgrave.jors.2600879>
610 [36] A. Mishra, S. Mukherjee, B. Merz, V.P. Singh, D.B. Wright, G. Villarini, S. Paul, D.N.
611 Kumar, C.P. Khedun, D. Niyogi, G. Schumann (2022), An Overview of Flood Concepts,
612 Challenges, and Future Directions, Journal of Hydrologic Engineering 27(6) 03122001,
613 Available from <https://doi.org/10.1061/(ASCE)HE.1943-5584.0002164>
614 [37] A.M. Mehta, A. Bruns, J. Newton (2017), Trust, but verify: social media models for disaster
615 management, Disasters 41(3) 549–565, Available from
616 <https://doi.org/10.1111/disa.12218>
617 [38] N. Kankanamge, T. Yigitcanlar, A. Goonetilleke, M. Kamruzzaman (2019), Can volunteer
618 crowdsourcing reduce disaster risk? A systematic review of the literature, International

619 Journal of Disaster Risk Reduction 35 101097, Available from
620 <https://doi.org/10.1016/j.ijdrr.2019.101097>
621 [39] Z. Song, H. Zhang, C. Dolan (2020), Promoting disaster resilience: Operation mechanisms
622 and self-organizing processes of crowdsourcing, Sustainability 12(5) 1862, Available from
623 <https://doi.org/10.3390/su12051862>
624 [40] S. Masud, D.F. Robinson, N. Sultana (2019), Factors influencing communities' flood risk
625 perceptions: outcome of a community survey in the Hawkesbury-Nepean Catchment,
626 Australia, Australasian Journal of Environmental Management 26(4) 407-425, Available
627 from <https://doi.org/10.1080/14486563.2019.1682077>
628 [41] National Weather Service Team (2014), National weather service central region
629 supplement 02-2002, Applicable to NWSI 10-922, Weather Forecast Office Hydrologic
630 Products Specification, Available from
631 <http://www.nws.noaa.gov/directives/sym/pd01009022c022002curr.pdf>
632 [42] R. E. Morss, K. J. Mulder, J. K. Lazo, J. L. Demuth (2016), How do people perceive,
633 understand, and anticipate responding to flash flood risks and warnings? Results from a
634 public survey in Boulder, Colorado, USA, Journal of Hydrology 541 649-664, Available
635 from <https://doi.org/10.1016/j.jhydrol.2015.11.047>
636 [43] J. van Alphen, E. van Beek (2006), From flood defence to flood management – Prerequisites
637 for sustainable flood management, Floods, from Defence to Management, Taylor & Francis
638 Group 11-15, London, Available from <https://doi.org/10.1201/9781439833513>
639 [44] E. Roy, J. Rousselle, J. Lacroix (2003), Flood damage reduction program (FDRP) in Quebec:
640 case study of the Chaudiere River, Natural Hazards 28 (2) 387–405, Available from
641 <https://doi.org/10.1023/A:1022942427248>

642 [45] R. J. Burby (2001), Flood insurance and floodplain management: the U.S. experience, Global
643 Environmental Change Part B: Environmental Hazards 3 (3) 111–122, Available from
644 <https://doi.org/10.3763/ehaz.2001.0310>
645 [46] Ø. A. Høydal, H. Berg, I. Haddeland, L. E. Petterson, A. Voksø, E. Øydvin (2000),
646 Procedures and guidelines for flood inundation maps in Norway, Potsdam, Germany 252-
647 261, Available from
648 <https://www.researchgate.net/publication/295650981_Procedures_and_guidelines_for_flo
649 od_inundation_maps_in_Norway>
650 [47] A. Gori, R. Blessing, A. Juan, S. Brody, P. Bedient (2019), Characterizing urbanization
651 impacts on floodplain through integrated land use, hydrologic, and hydraulic modeling,
652 Journal of Hydrology 568 82-95, Available from
653 <https://doi.org/10.1016/j.jhydrol.2018.10.053>
654 [48] H. Farahmand, S. Dong, A. Mostafavi (2021), Network analysis and characterization of
655 vulnerability in flood control infrastructure for system-level risk reduction, Computers,
656 Environment and Urban Systems 89 101663, Available from
657 <https://doi.org/10.1016/j.compenvurbsys.2021.101663>
658 [49] S. Dong, T. Yu, H. Farahmand, A. Mostafavi (2021), A hybrid deep learning model for
659 predictive flood warning and situation awareness using channel network sensors data,
660 Computer-Aided Civil and Infrastructure Engineering 36(4) 402-420, Available from
661 <https://doi.org/10.1111/mice.12629>
662 [50] M. Kamari, Y. Ham (2021), Vision-based volumetric measurements via deep learning-based
663 point cloud segmentation for material management in jobsites, Automation in Construction
664 121 103430, Available from < https://doi.org/10.1016/j.autcon.2020.103430>

[51] F. Cian, M. Marconcini, P. Ceccato, C. Giupponi (2018), Flood depth estimation by means of high-resolution SAR images and lidar data, Natural Hazards and Earth System Sciences 18(11) 3063-3084, Available from <https://doi.org/10.5194/nhess-18-3063-2018>

[52] V. Merwade, F. Olivera, M. Arabi, S. Edleman (2008), Uncertainty in flood inundation mapping: current issues and future directions, Journal of Hydrologic Engineering 13(7) 608-620, Available from <https://doi.org/10.1061/(ASCE)1084-0699(2008)13:7(608)>

[53] C. J. Ticehurst, P. Dyce, J. P. Guerschman (2009), Using passive microwave and optical remote sensing to monitor flood inundation in support of hydrologic modelling, Interfacing Modelling and Simulation with Mathematical and Computational Sciences, 18th World IMACS/MODSIM Congress 13-17, Available from <https://www.mssanz.org.au/modsim09/I10/ticehurst_I10.pdf>

[54] C. C. Sampson, A. M. Smith, P. D. Bates, J. C. Neal, M. A. Trigg (2016), Perspectives on open access high resolution digital elevation models to produce global flood hazard layers, Frontiers in Earth Science 3 85, Available from <https://doi.org/10.3389/feart.2015.00085>

[55] A. Ferro, D. Brunner, L. Bruzzone, G. Lemoine (2011), On the relationship between double bounce and the orientation of buildings in VHR SAR images, IEEE Geoscience and Remote Sensing Letters 8(4) 612-616, Available from <https://doi.org/10.1109/LGRS.2010.2097580>

[56] G. P. Asner (2001), Cloud cover in landsat observations in the Brazilian Amazon, International Journal of Remote Sensing 22 3855–3862, Available from <https://doi.org/10.1080/01431160010006926>

[57] M. Vojtek, A. Petroselli, J. Vojteková, S. Asgharinia (2019), Flood inundation mapping in small and ungauged basins: sensitivity analysis using the EBA4SUB and HEC-RAS

modeling approach, Hydrology Research 50 (4) 1002-1019, Available from <https://doi.org/10.2166/nh.2019.163>

[58] X. Shen, E.N. Anagnostou, G. H. Allen, G. R. Brakenridge, A. J. Kettner (2019), Near-real-time non-obstructed flood inundation mapping using synthetic aperture radar, Remote Sensing of Environment 221 302-315, Available from <https://doi.org/10.1016/j.rse.2018.11.008>

[59] P. Chaudhary, S. D'Aronco, J. P. Leitão, K. Schindler, J. D. Wegner (2020), Water level prediction from social media images with a multi-task ranking approach, ISPRS Journal of Photogrammetry and Remote Sensing 167 252-262, Available from <https://doi.org/10.1016/j.isprsjprs.2020.07.003>

[60] S. Park, F. Baek, J. Sohn, H. Kim (2021), Computer vision–based estimation of flood depth in flooded-vehicle images, Journal of Computing in Civil Engineering 35 (2) 04020072, Available from <https://doi.org/10.1061/(ASCE)CP.1943-5487.0000956>

[61] Hao, X., Lyu, H., Wang, Z., Fu, S., & Zhang, C. (2022), Detecting Spatial-temporal urban ponding distribution from surveillance videos based on computer vision, Research Square Preprint, Available from <https://doi.org/10.21203/rs.3.rs-1053795/v1>

[62] B. Alizadeh Kharazi, A. H. Behzadan (2021), Flood depth mapping in street photos with image processing and deep neural networks, Computers, Environment and Urban Systems, 88 101628, Available from <https://doi.org/10.1016/j.compenvurbsys.2021.101628>

[63] W. Liu, D. Anguelov, D. Erhan, C. Szegedy, S. Reed, C. Y. Fu, A. C. Berg (2016), SSD: Single shot multibox detector, In European Conference on Computer Vision 21-37, Springer, Cham, Available from <https://doi.org/10.1007/978-3-319-46448-0_2>

[64] C. Y. Fu, W. Liu, A. Ranga, A. Tyagi, A. C. Berg (2017), DSSD: Deconvolutional single shot detector, ArXiv Preprint, Available from <https://arxiv.org/abs/1701.06659>

[65] T. Y. Lin, P. Goyal, R. Girshick, K. He, P. Dollár (2017), Focal loss for dense object detection, In Proceedings of The IEEE International Conference on Computer Vision 2980-2988, Available from <https://openaccess.thecvf.com/content_ICCV_2017/papers/Lin_Focal_Loss_for_ICCV_2017_paper.pdf>

[66] T. Y. Lin, M. Maire, S. Belongie, J. Hays, P. Perona, D. Ramanan, P. Dollár, and C. L. Zitnick (2014), Microsoft COCO: Common objects in context, In European Conference on Computer Vision 740-755, Springer, Cham, Available from <https://doi.org/10.1007/978-3-319-10602-1_48>

[67] J. Redmon, S. Divvala, R. Girshick, A. Farhadi (2016), You Only Look Once: Unified, real-time object detection, In Proceedings of the IEEE Conference on Computer Vision and Pattern Recognition 779-788, Available from <https://www.cv-foundation.org/openaccess/content_cvpr_2016/papers/Redmon_You_Only_Look_CVPR_2016_paper.pdf>

[68] A. Bochkovskiy, C. Y. Wang, H. Y. M. Liao (2020), YOLOv4: Optimal speed and accuracy of object detection, ArXiv Preprint, Available from <https://arxiv.org/abs/2004.10934>

[69] J. Redmon, A. Farhadi (2018), YOLOv3: An incremental improvement, ArXiv Preprint, Available from <https://arxiv.org/abs/1804.02767>

[70] S. Liu, L. Qi, H. Qin, J. Shi, J. Jia (2018), Path aggregation network for instance segmentation, In Proceedings of the IEEE Conference on Computer Vision and Pattern Recognition 8759–68, Available from <

https://openaccess.thecvf.com/content_cvpr_2018/papers/Liu_Path_Aggregation_Network_CVPR_2018_paper.pdf>

[71] T. J. Cova, J. P. Johnson (2003), A network flow model for lane-based evacuation routing. Transportation research part A: Policy and Practice 37(7) 579-604, Available from <https://doi.org/10.1016/S0965-8564(03)00007-7>

[72] A. Stepanov, J.M. Smith (2009), Multi-objective evacuation routing in transportation networks, European Journal of Operational Research 198(2) 435-446, Available from <https://doi.org/10.1016/j.ejor.2008.08.025>

[73] H. Lim Jr, M.B. Lim, M. PIANTANAKULCHAI (2013), A review of recent studies on flood evacuation planning, Journal of the Eastern Asia Society for Transportation Studies 10 147-162, Available from <https://doi.org/10.11175/easts.10.147>

[74] M. He, C. Chen, F. Zheng, Q. Chen, J. Zhang, H. Yan, Y. Lin (2021), An efficient dynamic route optimization for urban flooding evacuation based on cellular automata, Computers, Environment and Urban Systems, 87 101622, Available from <https://doi.org/10.1016/j.compenvurbsys.2021.101622>

[75] R. Gomes, J. Straub (2017), Genetic algorithm for flood detection and evacuation route planning, In Algorithms and Technologies for Multispectral, Hyperspectral, and Ultraspectral Imagery XXIII 10198 384, SPIE, Available from <https://doi.org/10.1117/12.2266474>

[76] X. Wang, X. Wang, J. Zhai, X. Li, H.Huang, C. Li, J. Zheng, H. Sun (2017), Improvement to flooding risk assessment of storm surges by residual interpolation in the coastal areas of Guangdong Province, China, Quaternary International, 453 1-14, Available from <https://doi.org/10.1016/j.quaint.2016.12.025>

[77] C. Viavattene, D. Fadipe, J. Old, V. Thompson, K. Thorburn (2022), Estimation of Scottish pluvial flooding Expected Annual Damages using interpolation techniques, Water 14(3) 308, Available from <https://doi.org/10.3390/w14030308>

[78] Huang, X., Wang, C. and Li, Z. (2018), A near real-time flood-mapping approach by integrating social media and post-event satellite imagery, Annals of GIS, 24(2) 113-123, Available from <https://doi.org/10.1080/19475683.2018.1450787>

[79] O. L. Huibregtse, M. C. Bliemer, S.P. Hoogendoorn (2010), Analysis of near-optimal evacuation instructions, Procedia Engineering 3 189-203, Available from <https://doi.org/10.1016/j.proeng.2010.07.018>

[80] F. Sayyady, S. D. Eksioglu (2010), Optimizing the use of public transit system during no-notice evacuation of urban areas, Computers and Industrial Engineering 59 (4) 488-495, Available from <https://doi.org/10.1016/j.cie.2010.06.001>

[81] G. B. Dantzig, J. H. Ramser (1959), The truck dispatching problem, Management Science 6(1) 80–91, Available from <https://doi.org/10.1287/mnsc.6.1.80>

[82] Q. Lu (2006), Capacity constrained routing algorithms for evacuation route planning. University of Minnesota, Available from <https://hdl.handle.net/11299/215702>

[83] P. Hart, N. Nilsson, B., Raphael (1968), A Formal Basis for the Heuristic Determination of Minimum Cost Paths, IEEE Transactions on Systems Science and Cybernetics 4(2) 100–107, Available from <https://doi.org/10.1109/tssc.1968.300136>

[84] A. S. Berens, A.S., T. Palmer, N. D. Dutton, A. Lavery, M. Moore (2021), Using search-constrained inverse distance weight modeling for near real-time riverine flood modeling: Harris County, Texas, USA before, during, and after Hurricane Harvey, Natural Hazards 105(1) 277-292, Available from <https://doi.org/10.1007/s11069-020-04309-w>

779 [85] C. Marche, G. Lessard, B. El Gharbi (1990), Kriging technique for river flood representation,
780 Journal of Hydraulic Research 28(5) 629-643, Available from
781 <https://doi.org/10.1080/00221689009499051>
782 [86] X. Sun, R. G. Mein, T. D. Keenan, J. F. Elliott (2000), Flood estimation using radar and
783 raingauge data, Journal of Hydrology 239(1-4) 4-18, Available from
784 <https://doi.org/10.1016/S0022-1694(00)00350-4>
785 [87] K. Chokmani, T. B. Ouarda (2004), Physiographical space-based kriging for regional flood
786 frequency estimation at ungauged sites, Water Resources Research 40(12), Available from
787 <https://doi.org/10.1029/2003WR002983>.
788 [88] M. K. Nezhad, K. Chokmani, T. B. Ouarda, M. Barbet, P. Bruneau (2010), Regional flood
789 frequency analysis using residual kriging in physiographical space, Hydrological Processes
790 24(15) 2045-2055, Available from <https://doi.org/10.1002/hyp.7631>
791 [89] K. Zhang, D. Gann, M. Ross, Q. Robertson, J. Sarmiento, S. Santana, J. Rhome, C. Fritz
792 (2019), Accuracy assessment of ASTER, SRTM, ALOS, and TDX DEMs for Hispaniola and
793 implications for mapping vulnerability to coastal flooding, Remote Sensing of Environment
794 225 290-306, Available from <https://doi.org/10.1016/j.rse.2019.02.028>
795 [90] B. M. Newman, P. R. Newman (2017), Development through life: A psychosocial approach
796 [edition missing], Cengage Learning EMEA, Available from
797 <https://www.perlego.com/book/2754529/development-through-life-a-psychosocial-
798 approach-pdf>
799 [91] D. Sandink, S. P. Simonovic, A. Schardong, R. Srivastav (2016), A decision support system
800 for updating and incorporating climate change impacts into rainfall intensity-duration-

frequency curves: Review of the stakeholder involvement process, Environmental Modelling and Software 84 193-209, Available from <https://doi.org/10.1016/j.envsoft.2016.06.012>

[92] J. Saldaña (2009), The coding manual for qualitative researchers, SAGE Publications Ltd 3.

[93] S. Ruby, D. B. Copeland, D. Thomas (2020), Agile web development with rails 6, Pragmatic Bookshelf.

[94] S. Aggarwal (2018), Modern web-development using ReactJS, International Journal of Recent Research Aspects 5(1) 133-137, Available from <http://ijrra.net/Vol5issue1/IJRRA-05-01-27.pdf>

[95] U.S. Department of Transportation (2009), Federal highway Administration, Manual On Uniform Traffic Control Devices for Streets and Highways, Available from <https://mutcd.fhwa.dot.gov/pdfs/2009r1r2/mutcd2009r1r2edition.pdf>

[96] D. P. Kingma, J. Ba, Adam (2014): A method for stochastic optimization, ArXiv Preprint, Available from <https://arxiv.org/abs/1412.6980>

[97] E.W. Dijkstra (1959), A note on two problems in connexion with graphs, Numerische Mathematik, 1(1) 269–271, Available from <https://ir.cwi.nl/pub/9256/9256D.pdf>

[98] K. Krivoruchko (2012), Empirical Bayesian kriging, ArcUser Fall 6(10), Available from <https://www.esri.com/NEWS/ARCUSER/1012/files/ebk.pdf>

[99] A. Gupta, T. Kamble, D. Machiwal (2017), Comparison of ordinary and Bayesian kriging techniques in depicting rainfall variability in arid and semi-arid regions of north-west India, Environmental Earth Sciences 76(15) 1-16, Available from <https://doi.org/10.1007/s12665-017-6814-3>

[100] M. F. Goodchild (2009), What problem? Spatial autocorrelation and geographic information science, Geographical Analysis 41(4) 411-417, Available from <https://doi.org/10.1111/j.1538-4632.2009.00769.x>

[101] F. Giustini, G. Ciotoli, A. Rinaldini, L. Ruggiero, M. Voltaggio (2019), Mapping the geogenic radon potential and radon risk by using Empirical Bayesian Kriging regression: A case study from a volcanic area of central Italy, Science of the Total Environment 661 449-464, Available from <https://doi.org/10.1016/j.scitotenv.2019.01.146>

[102] National Weather Service Internet Services Team (2021), National Weather Service - Water, Available from <https://water.weather.gov/ahps/>

[103] ArcGIS Developer (2021), ArcGIS API for Python, Available from <https://developers.arcgis.com/python/>

[104] H. Garcia-Molina, M. Joglekar, A. Marcus, A. Parameswaran, V. Verroios (2016), Challenges in data crowdsourcing, IEEE Transactions on Knowledge and Data Engineering 28(4) 901-911, Available from <https://doi.org/10.1109/TKDE.2016.2518669>

[105] J.E. O'Connor, J.E. Costa (2004), Spatial distribution of the largest rainfall-runoff floods from basins between 2.6 and 26,000 km2 in the United States and Puerto Rico, Water Resources Research 40(1), Available from <https://doi.org/10.1029/2003WR002247>

[106] L. Alfieri, P. Salamon, A. Bianchi, J. Neal, P. Bates, L. Feyen (2014), Advances in pan-European flood hazard mapping, Hydrological processes 28(13) 4067-4077, Available from <https://doi.org/10.1002/hyp.9947>

[107] D.Z. Sui, R.C. Maggio (1999), Integrating GIS with hydrological modeling: practices, problems, and prospects, Computers, Environment and Urban systems 23(1) 33-51, Available from <https://doi.org/10.1016/S0198-9715(98)00052-0>

[108] I.C. Overton (2005) Modelling floodplain inundation on a regulated river: integrating GIS, remote sensing and hydrological models, River Research and Applications 21(9) 991-1001, Available from <https://doi.org/10.1002/rra.867>

Step 1: Community needs assessment survey

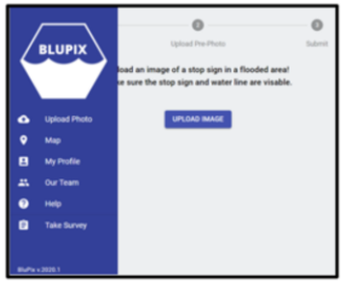

Step 2: Designing the evacuation decision support platform

Crowdsourced data collection

Paired photos

Stop sign and pole detection

Pole length calculation

Flood depth estimation

$$P'_{in}: \frac{30_{in}}{S'_{pix}} \times P'_{pix}$$

$$P_{in}: \frac{30_{in}}{S_{pix}} \times P_{pix}$$

$$D_{in} = P_{in} - P'_{in}$$

1 2 3 4 5

Step 3: Enhanced flood depth mapping

Augmenting live stream gauge data

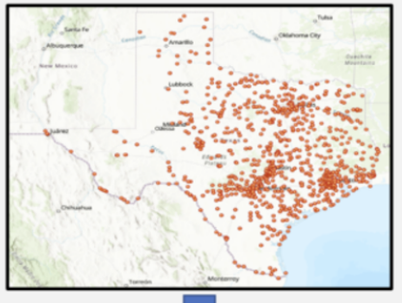

Flood inundation mapping

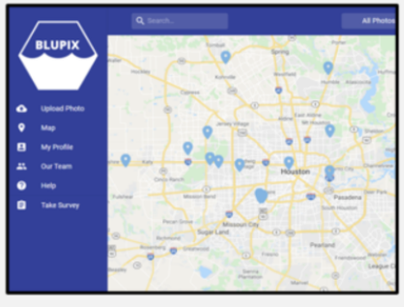

Determining shortest flood-free route

Step 4: Risk-informed route optimization

BLUPIX

- Upload Photo
- Map
- My Profile
- Our Team
- Help
- Take Survey

Search...

All Photos

Today 1 Week 1 Month 6 Months 1 Year 1+ Years

Paired

Needs Pairing

5063 Dumfries Dr, Houston, TX 77096, USA
(29.671526, -95.469196)

Post-Flood Image

Date: Unknown

Flood Height: 32.58

Source: File Upload

SEE THIS ON GOOGLE STREETVIEW

Houston

BluPix v.2020.1

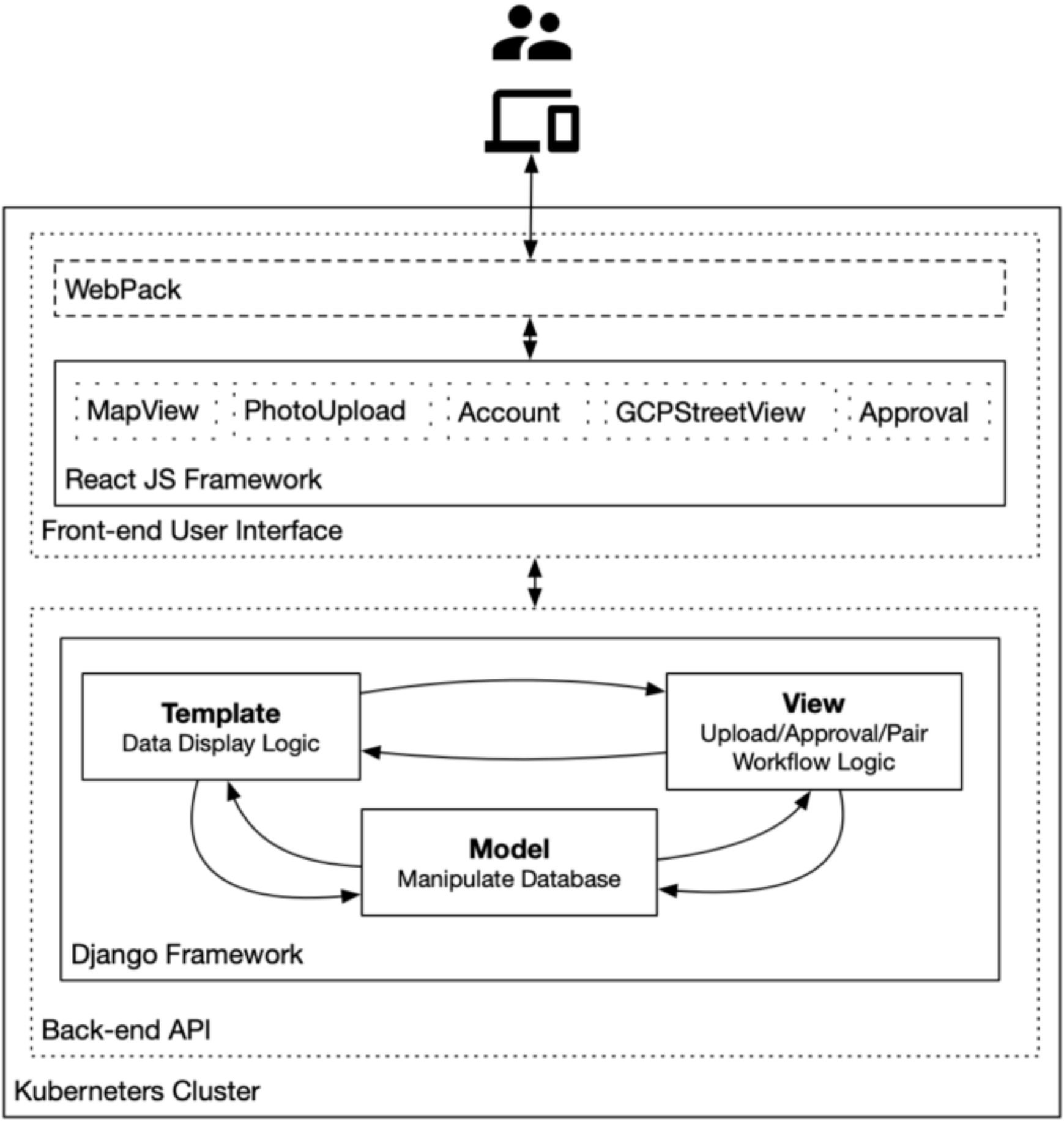
WebPack
MapView
PhotoUpload
Account
GCPStreetView
Approval
React JS Framework
Front-end User Interface
Template
Data Display Logic
View
Upload/Approval/Pair
Workflow Logic
Model
Manipulate Database
Django Framework
Back-end API
Kuberneters Cluster

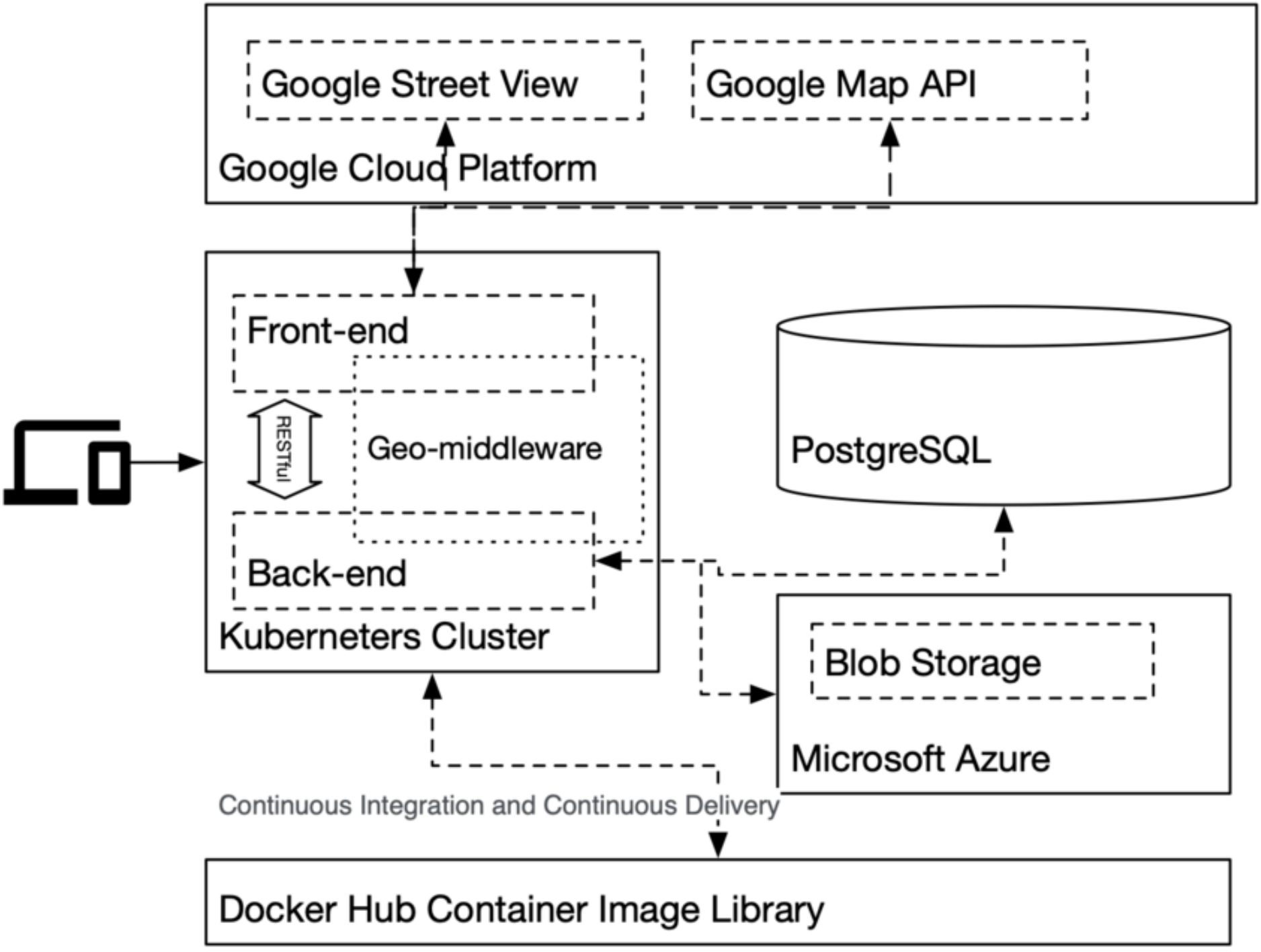
Google Street View
Google Map API
Google Cloud Platform
Front-end
RESTful
Geo-middleware
Back-end
Kuberneters Cluster
PostgreSQL
Blob Storage
Microsoft Azure
Continuous Integration and Continuous Delivery
Docker Hub Container Image Library

Pre-flood photo

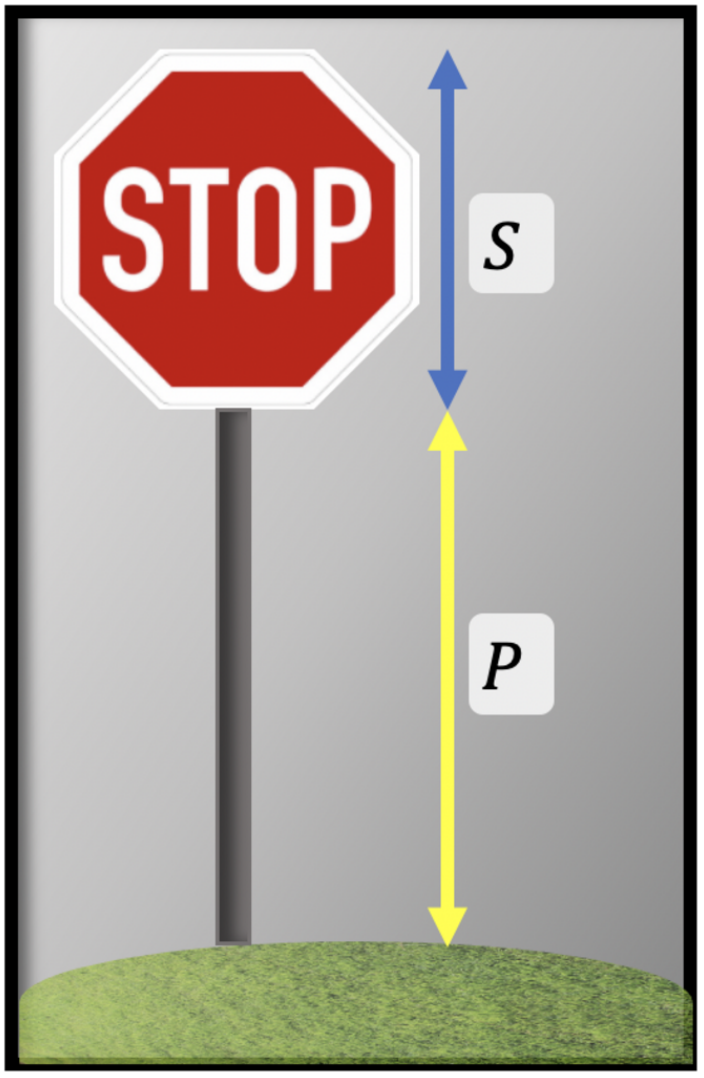

Post-flood photo

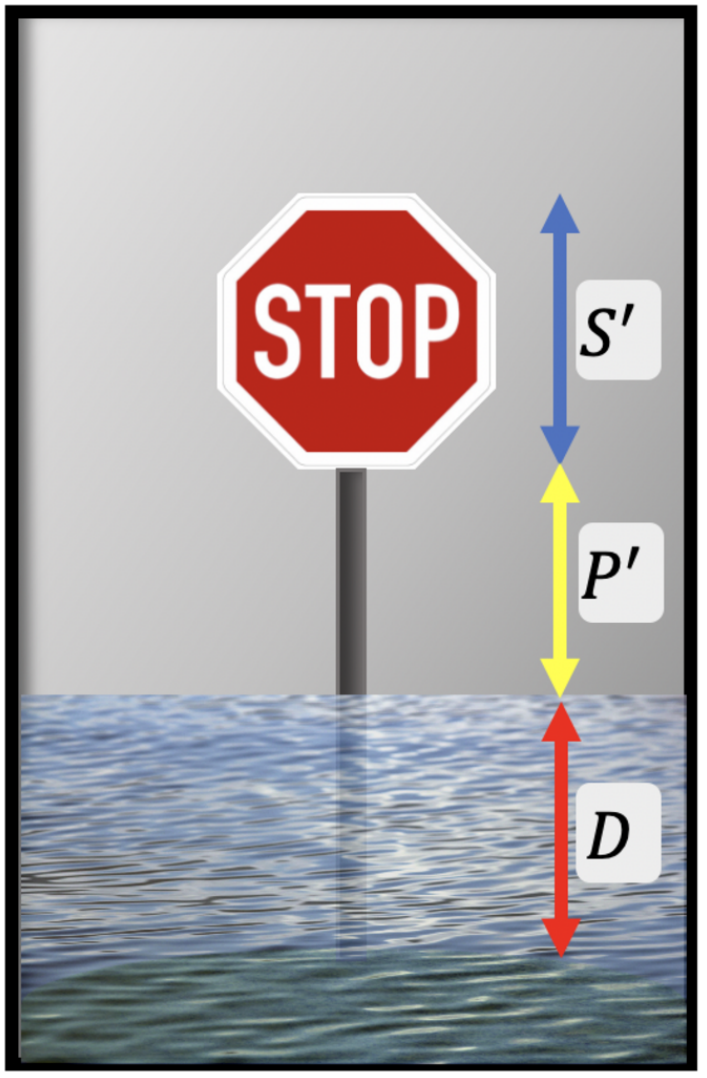

Paired

$$P\ (in) = \frac{30\ (in)}{S\ (pix)} \times P\ (pix)$$

Pre-flood pole length

$$P'\ (in) = \frac{30\ (in)}{S'(pix)} \times P'(pix)$$

Post-flood pole length

$$D\ (in) = P\ (in) - P'(in)$$

Floodwater depth

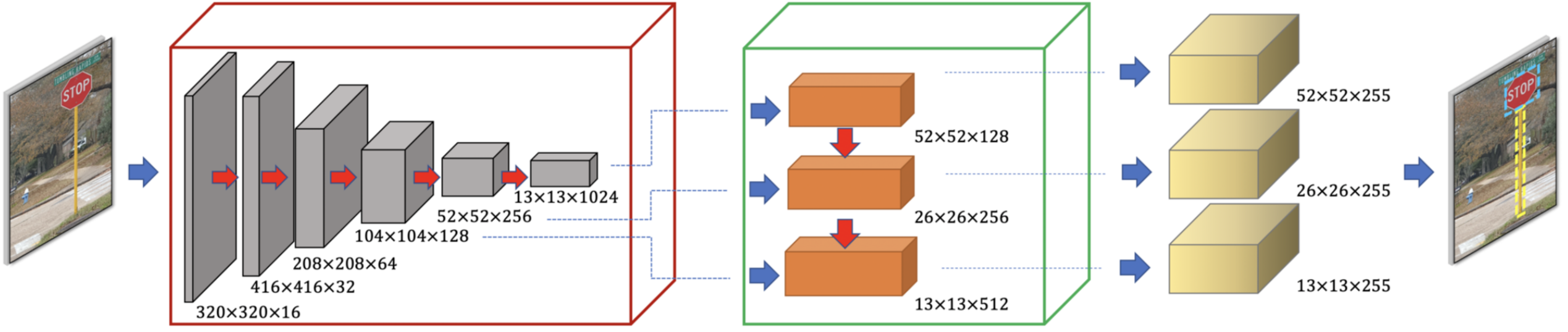

Input:
320×320×3
image

Backbone:
CSPDarknet53

Neck:
SPP, PANet

Head:
YOLOv3

Output:
Bounding boxes of
recognized classes

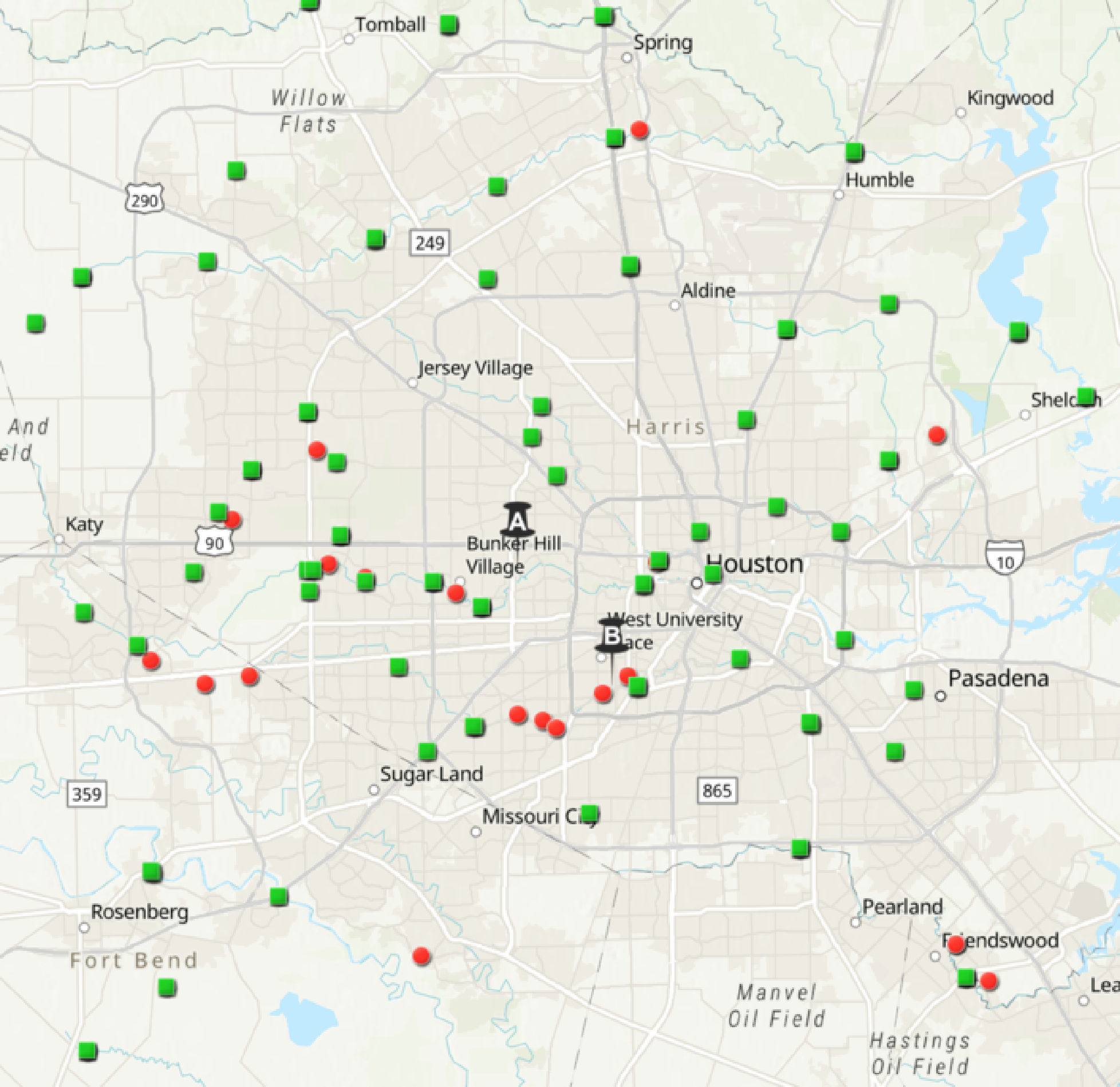
Tomball
Spring
Willow
Flats
Kingwood
Humble
290
249
Aldine
Jersey Village
Harris
Katy
90
A
Bunker Hill
Village
Houston
10
West University
Place
B
Pasadena
Sugar Land
359
865
Missouri City
Rosenberg
Fort Bend
Pearland
Manvel
Oil Field
Hastings
Oil Field

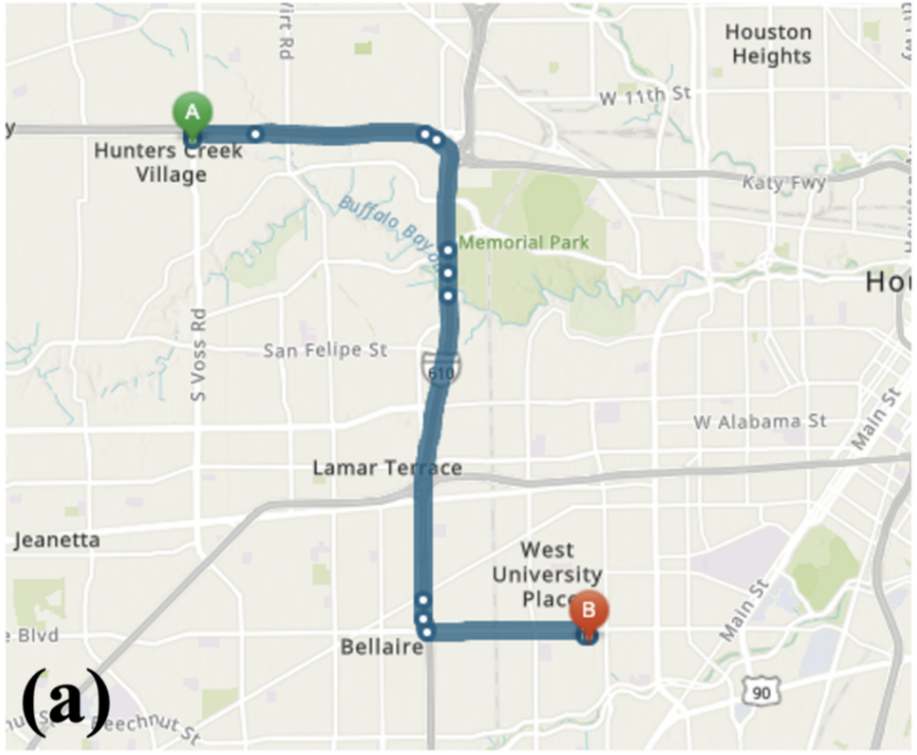
Houston Heights
W 11th St
A
Hunters Creek Village
Katy Fwy
Buffalo Bayou
Memorial Park
S Voss Rd
San Felipe St
610
W Alabama St
Main St
Lamar Terrace
Jeanetta
West University Place
B
Bellaire
Beechnut St
90
(a)

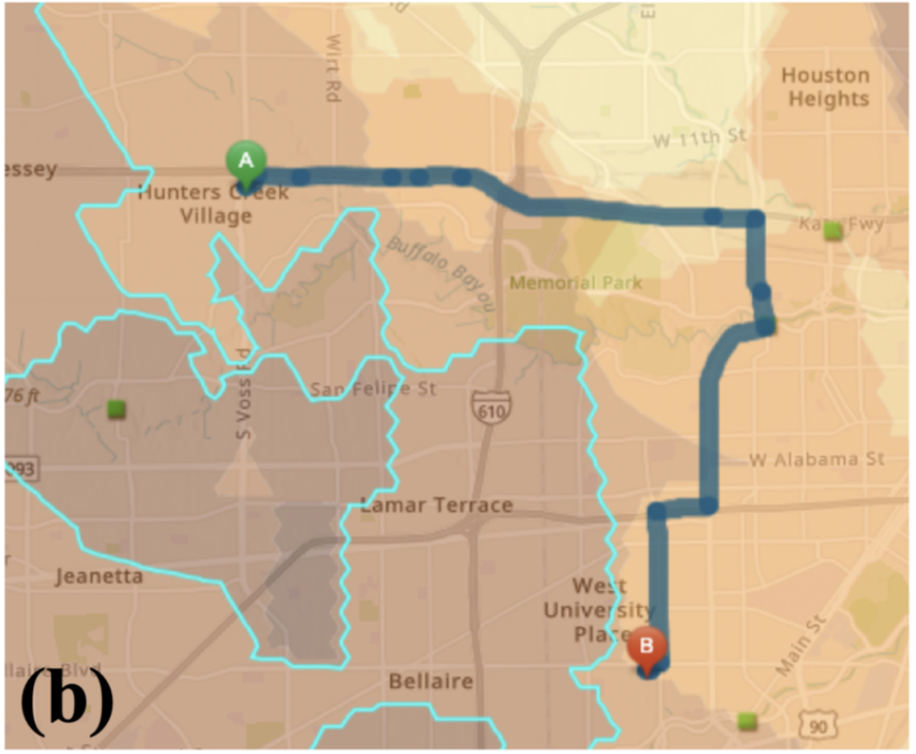
Houston Heights
W 11th St
A
Hunters Creek Village
Buffalo Bayou
Memorial Park
S Voss Rd
San Felipe St
610
W Alabama St
Lamar Terrace
Jeanetta
West University Place
B
Bellaire
Main St
90
(b)

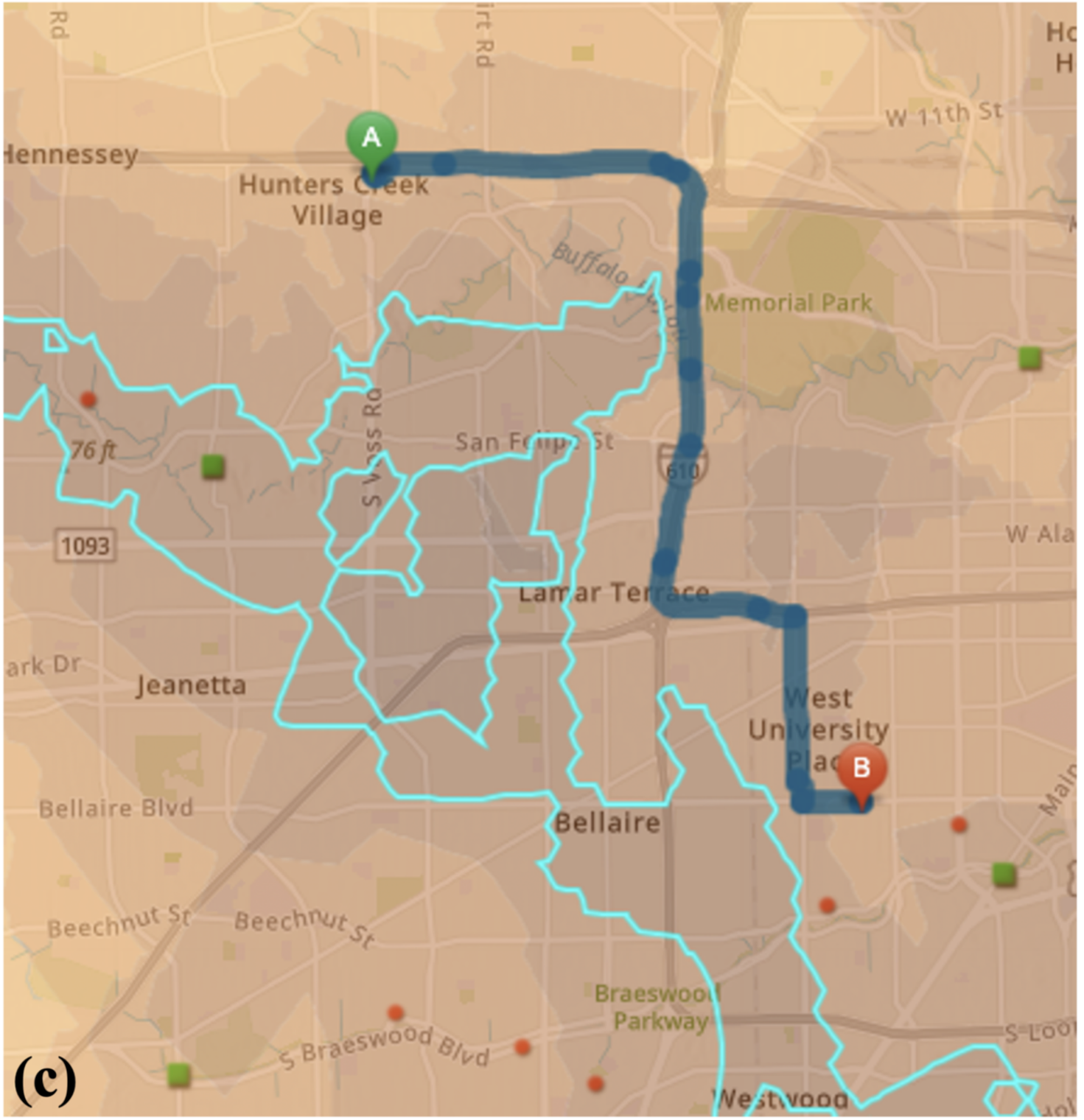
W 11th St
A
Hunters Creek Village
Memorial Park
76 ft
S Voss Rd
San Felipe St
610
1093
Lamar Terrace
Jeanetta
West University Place
B
Bellaire Blvd
Bellaire
Beechnut St
Beechnut St
Braeswood Parkway
S Braeswood Blvd
(c)

Table 1. *Performance of the trained YOLOv4 model on 20 selected paired photos in Hurricane Harvey (August 27 – September 1, 2017) in Houston, Texas. (S=stop sign; P=pole)*

Metric	Class	Pre-flood (*n*=20)	Post-flood (*n*=20)	All photos (n=40)
Average IoU (%)	S+P	83.10	79.69	81.44
Precision @ 0.25 conf (%)	S+P	93	93	93
Recall @ 0.25 conf (%)	S+P	100	95	98
AP (%)	S	100	100	100
	P	100	92.30	96.54
mAP @ 0.50 (%)	S+P	100	96	98.27
Average detection time (sec)	S+P	0.10	0.10	0.10
MAE of pole length estimation (in.)	P	2.73	2.64	3.80

Table 2. *Comparison of three routing scenarios in the experiment area.*

Metric	Scenario (a)	Scenario (b)	Scenario (C)
Estimated travel time (driving) (min.)	22	26	22
Total travel distance (miles)	9.99	11.53	9.60